Vibroacoustic modeling of submerged stiffened cylindrical shells with internal structures under random excitations

Valentin Meyer, Laurent Maxit, Ygäal Renou, Christian Audoly

inter.noise
HAMBURG 2016

Vibroacoustic modeling of submerged stiffened cylindrical shells with internal structures under random excitations

Valentin MEYER[1,2]; Laurent MAXIT[1]; Ygaal RENOU[2]; Christian AUDOLY[2]
[1]Univ Lyon, INSA-Lyon, LVA EA677, France
[2]DCNS Research, France

ABSTRACT
The vibroacoustic behavior of a structure excited by a partially space-correlated random pressure fields such as turbulent boundary layers or internal diffuse fields is of great interest for aeronautical or naval applications. Many works have been carried out for structures such as plates or simple cylinders whereas little attention has been paid on more complex cases. The aim of this paper is to study this problem for a ribbed cylindrical shell coupled to internal structures. The proposed modeling is based on the combination of two methods developed recently by the authors: the wavenumber-point (k, M) reciprocity technique and the Condensed Transfer Function (CTF) method. The first one estimates the sensitivity functions at point M of the system from its vibratory velocity field induced by a point excitation at M. This velocity field is estimated with the second method. The CTF method is a substructuring approach which consists in coupling a semi-analytical model of a submerged cylindrical shell with Finite Element models of axisymmetric (ribs, bulkheads) and non-axisymmetric (floor partitions, engine foundations) internal frames. A numerical example of a submerged stiffened cylindrical shell excited by random pressure fields will be given and the influence of the internal frames will be discussed.

Keywords: Vibroacoustics, Cylindrical shell, Diffuse Sound Field, Turbulent boundary layer
I-INCE Classification of Subjects Numbers: 54.3, 76.9

1. INTRODUCTION

In many aeronautical or naval applications, ribbed structures are subject to random pressure fields such as Diffuse Sound Fields (DSF) or fluctuations due to the turbulent flow induced by their movement. These excitations yield vibrations, which knowledge is of primarily importance in practice. Many works can be found in the literature for plates under a Turbulent Boundary Layer (TBL). Strawderman [1] reviews the first existing models of finite and infinite plates. He points out that none of the models fully agrees with experimental results but that the ones for the finite plate performs better. The complexity of the problem is successively increased by taking heavy fluid loading into account [2, 3] or by stiffening the plates [4]. Maxit and Denis [5] use the wavevector-frequency analysis, earlier reviewed by Strawderman [6], and the reciprocity principle to study the problem of a ribbed plate with heavy fluid loading. Their method consists in determining the second order moment of the response thanks to the wall pressure fluctuations and the sensistivity functions of the system. The sensitivity function at a point M of the system is estimated from the vibratory field induced by a point excitation at M. As the formulation of this method is not only valid for plates, the aim of the present work is to apply it to the case of submerged cylindrical shells with internal structures. Nevertheless, the aim of this paper is not to characterize the TBL on a circular cylinder and widespread models models such as Corcos' [7] or Chase's [8] will be used because of their simplicity of implementation. Indeed, in the case where the TBL thickness is small compared with the radius of curvature of the system, which is the case in this study, the boundary layer is similar to a planar one [9, 10].

A substructuring method is used to determine the sensitivity functions of the submerged cylindrical shell with internal structures. The Condensed Transfer Function (CTF) method, previously developed by the authors [11, 12], is an extension of the classical admittance approach [13] to allow coupling along lines. A set of orthonormal functions called condensation functions is used as a basis for approximating the displacements

[1]email: valentin.meyer@insa-lyon.fr

and the forces at the junctions between the subsystems. Condensed transfer functions are then defined and calculated for each uncoupled subsystems, and the superposition principle for passive linear systems leads to the vibroacoustic behavior of the coupled system. One of the main advantage of the CTF method is that the condensed transfer functions of the uncoupled subsystems can be described by different methods. In this case, the submerged shell CTFs are calculated by solving the Flügge equations in the spectral domain, whereas the internal frames are modeled by FEM, allowing flexibility on their geometry.

The paper is organized as follows:

- Section 2 presents the wavenumber-point (k,M) reciprocity technique.
- In section 3, the CTF method is applied to calculate the sensitivity functions of a submerged cylindrical shell with internal structures.
- An application to a complex cylinder under a DSF and a TBL is proposed in section 4. The influence of non-axisymmetric internal frames will be discussed.
- Conclusions are drawn in section 5.

2. THE WAVENUMBER-FREQUENCY (k, M) RECIPROCITY TECHNIQUE

This section is based on the wavenumber-frequency formulation which can be found in the literature [3, 6, 14]. The wavenumber-frequency (k, M) reciprocity technique has been presented in details by Maxit and Denis [5] and the general outline is briefly described in this section.

Let us consider a vibroacoustic system made of a structure coupled to a fluid domain. The surface Σ_p is excited by a random pressure field. The wall pressure $p_b(\tilde{\mathbf{x}}, t)$ is expressed in a point $\tilde{\mathbf{x}} \in \Sigma_p$ as a function of the time t. The system is supposed to be linear and invariant in time, so that the displacement w at a point $\mathbf{x}$ can be expressed as:

$$w(\mathbf{x}, t) = \int_{\Sigma_p} \int_{-\infty}^{+\infty} h_w\left(\mathbf{x}, \tilde{\mathbf{x}}, t - \tilde{\tau}\right) p_b\left(\tilde{\mathbf{x}}, \tilde{\tau}\right) \mathrm{d}\tilde{\tau} \mathrm{d}\tilde{\mathbf{x}} \tag{1}$$

where $h_w\left(\mathbf{x}, \tilde{\mathbf{x}}, t\right)$ is the impulse response of the system at point $\mathbf{x}$ when excited by an impulse unitary force at point $\tilde{\mathbf{x}}$.

The excitation being random, the quantity of interest is the second order moment of the displacement. Considering that the random process is ergodic, the inter-correlation function $R_{ww}(\mathbf{x}, \mathbf{x}', t)$ is defined as:

$$R_{ww}(\mathbf{x}, \mathbf{x}', t) = \int_{-\infty}^{+\infty} w(\mathbf{x}, \tau) w(\mathbf{x}', t + \tau) \mathrm{d}\tau \tag{2}$$

Injecting Eq. (1) into Eq. (2) and applying a Fourier transform in the time domain yields the space-frequency-spectrum $S_{ww}(\mathbf{x}, \mathbf{x}', f)$:

$$S_{ww}(\mathbf{x}, \mathbf{x}', f) = \int_{\Sigma_p} \int_{\Sigma_p} H_w^*\left(\mathbf{x}, \tilde{\mathbf{x}}, f\right) S_{pp}\left(\tilde{\mathbf{x}}, \tilde{\tilde{\mathbf{x}}}, f\right) H_w\left(\mathbf{x}', \tilde{\tilde{\mathbf{x}}}, f\right) \mathrm{d}\tilde{\mathbf{x}} \mathrm{d}\tilde{\tilde{\mathbf{x}}} \tag{3}$$

where $H_w\left(\mathbf{x}, \tilde{\mathbf{x}}, f\right)$ is the transfer function in displacement of point $\mathbf{x}$ when excited at point $\tilde{\mathbf{x}}$, $S_{pp}\left(\tilde{\mathbf{x}}, \tilde{\tilde{\mathbf{x}}}, f\right)$ is the space-frequency spectrum of the wall pressure, and * denotes the conjugate.

The space Fourier transform of $S_{pp}\left(\tilde{\mathbf{x}}, \tilde{\tilde{\mathbf{x}}}, f\right)$ can be written as a function of the wavenumber-frequency spectrum of the wall pressure $\phi_{pp}(\mathbf{k}, f)$:

$$S_{pp}\left(\tilde{\mathbf{x}}, \tilde{\tilde{\mathbf{x}}}, f\right) = \frac{1}{(2\pi)^2} \iint_{-\infty}^{+\infty} \phi_{pp}(\mathbf{k}, f) e^{-j\mathbf{k}(\tilde{\tilde{\mathbf{x}}} - \tilde{\mathbf{x}})} \mathrm{d}^2\mathbf{k} \tag{4}$$

$\phi_{pp}(\mathbf{k}, f)$ is a power spectrum density that characterizes the excitation and is supposed to be known. This value is expressed in Pa^2.s and is defined for positive frequencies only. Let us define $\tilde{H}_w(\mathbf{x}, \mathbf{k}, f)$ as the frequency response at point $\mathbf{x}$ when the system is excited by a plane wave with wavevector $\mathbf{k}$:

$$\tilde{H}_w(\mathbf{x}, \mathbf{k}, f) = \int_{\Sigma_p} H_w\left(\mathbf{x}, \tilde{\mathbf{x}}, f\right) e^{j\mathbf{k}\tilde{\mathbf{x}}} \mathrm{d}\tilde{\mathbf{x}} \tag{5}$$

Thus, injecting Eq. (4) into Eq. (3) and using Eq. (5), the space-frequency spectrum of displacement can be written finally as:

$$S_{ww}(\mathbf{x},\mathbf{x}',f) = \frac{1}{4\pi^2}\iint_{-\infty}^{+\infty} \tilde{H}_w^*(\mathbf{x},\mathbf{k},f)\phi_{pp}(\mathbf{k},f)\tilde{H}_w(\mathbf{x}',\mathbf{k},f)\mathrm{d}^2\mathbf{k} \tag{6}$$

If one is interested only in the spectral power density of the displacement at point $\mathbf{x}$ (*i.e.* $\mathbf{x} = \tilde{\mathbf{x}}$), Eq. (6) can be written as follows:

$$S_{ww}(\mathbf{x},f) = \frac{1}{4\pi^2}\iint_{-\infty}^{+\infty} |\tilde{H}_w(\mathbf{x},\mathbf{k},f)|^2\phi_{pp}(\mathbf{k},f)\mathrm{d}^2\mathbf{k} \tag{7}$$

The same developments can be made for the spectral power density of the pressure at point $\mathbf{z}$:

$$S_{pp}(\mathbf{z},f) = \frac{1}{4\pi^2}\iint_{-\infty}^{+\infty} |\tilde{H}_p(\mathbf{z},\mathbf{k},f)|^2\phi_{pp}(\mathbf{k},f)\mathrm{d}^2\mathbf{k} \tag{8}$$

where $\tilde{H}_p(\mathbf{z},\mathbf{k},f)$ represents the pressure at point $\mathbf{z}$ in the fluid when the system is excited by a plane wave of wavevector $\mathbf{k}$. It should be noted that this plane wave can be either propagating either evanescent, depending on its value compared to the acoustic wavenumber $k_0 = \frac{2\pi f}{c_0}$, with c_0 the sound velocity.

When solving a problem numerically, integrals over infinite domains such as in Eqs. (7) and (8) are an issue. However, it can be shown on systems such as plates or shells that the transfer functions $\tilde{H}_w(\mathbf{x},\mathbf{k},f)$ and $\tilde{H}_p(\mathbf{z},\mathbf{k},f)$ tend to 0 when $|\mathbf{k}| \to \infty$. Thus, a cutoff wavenumber $\mathbf{N_k}$ based on the response function of the system along the wavenumbers can be defined [5], allowing the integration domain to be truncated. The difficulty now lies in the calculation of the transfer functions over the integration domain. In practice, it consists in determining the displacement at location $\mathbf{x}$ or the pressure at location $\mathbf{z}$ when the system is excited by all the wavenumbers included in the integration domain. The number of excitations can thus be large and leads to prohibitive computation time. To tackle this issue, the use of the Lyamshev reciprocity principle is proposed [15]. It consists in exploiting the property that the transfer function between two points remains the same if the observation and excitation point are exchanged:

$$H_w\left(\mathbf{x},\tilde{\mathbf{x}},f\right) = H_w\left(\tilde{\mathbf{x}},\mathbf{x},f\right) \tag{9}$$

Eq. (5) can thus be written:

$$\tilde{H}_w(\mathbf{x},\mathbf{k},f) = \int_{\Sigma_p} H_w\left(\tilde{\mathbf{x}},\mathbf{x},f\right)e^{j\mathbf{k}\tilde{\mathbf{x}}}\mathrm{d}\tilde{\mathbf{x}} \tag{10}$$

This equivalence is called the wavenumber-point (k, M) reciprocity principle. It means that the power spectrum density of the displacement of the system at point $\mathbf{x}$ can be calculated through Eq. (7), knowing the vibratory field of the system excited by a point force at point $\mathbf{x}$. Similarly, the Lyamshev reciprocity principle is also valid for a point $\mathbf{z}$ in the fluid domain. The pressure at point $\mathbf{z}$ for a point force at $\mathbf{x}$ is equal to the displacement at point $\mathbf{x}$ when the system is excited by an acoustic monopole at point $\mathbf{z}$. Hence, the power spectrum density of the pressure at point $\mathbf{z}$ can be determined through Eq. (8), knowing the vibratory field of the system excited by a monopole in $\mathbf{z}$.

This paper focuses on the response of stiffened cylindrical shells with internal structures under random excitation. The reciprocity technique is illustrated for such a system in Fig. 1. In this case, the calculation of the power spectrum densities of displacement $\tilde{H}_w(\mathbf{x},\mathbf{k},f)$ and of pressure $\tilde{H}_p(\mathbf{z},\mathbf{k},f)$ used in Eq. (7) and (8) is not straightforward. Therefore, the Condensed Transfer Function (CTF) method presented in the next section is used to tackle this issue.

3. APPLICATION OF THE CONDENSED TRANSFER FUNCTION METHOD

3.1 Principle of the method

The Condensed Transfer Function (CTF) method is a substructuring method where the subsystems are modeled by plates and shells and coupled along lines [11]. On each junction between subsystems, a set of orthonormal functions $(\varphi_n(s))_{1\geq n\geq N}$ called *condensation functions* is defined, where s is the curvilinear

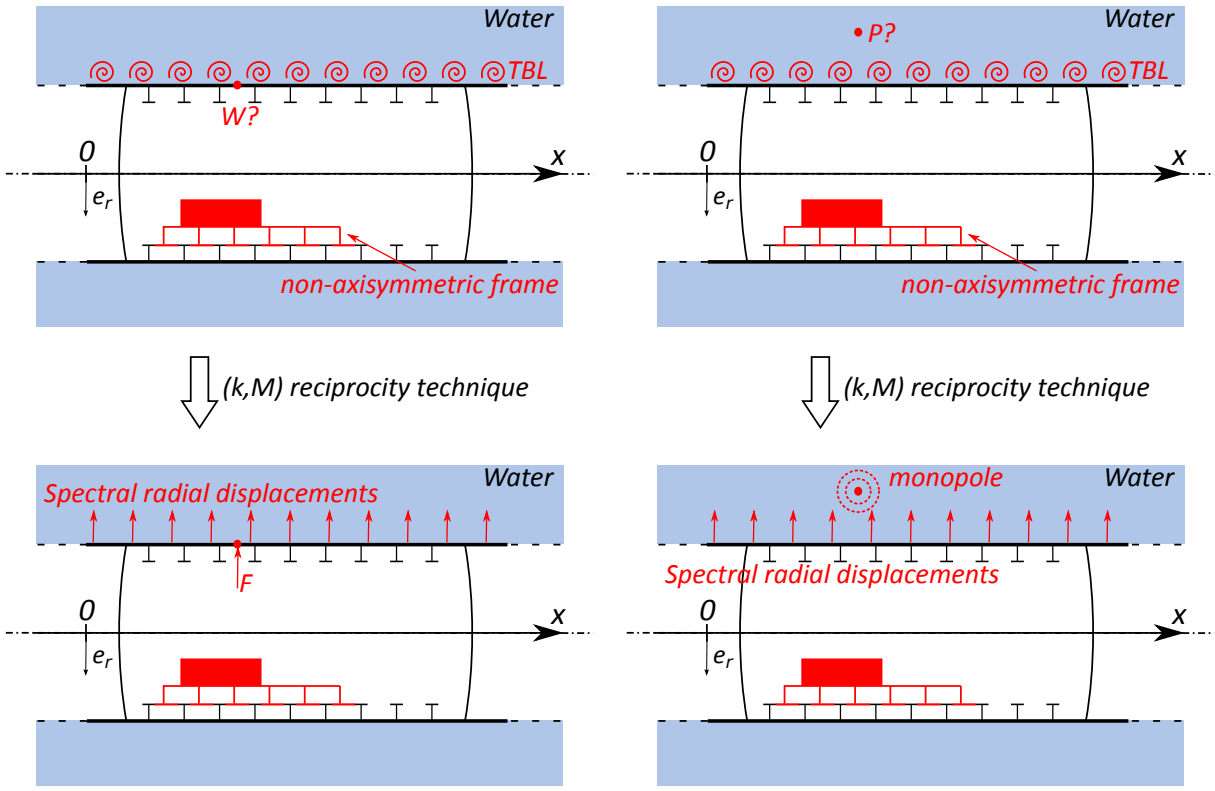

(a) (b)

Figure 1: The (k, M) reciprocity technique applied to a stiffened submerged cylindrical shell with internal structures to evaluate (a) the displacement at a point on the shell surface or (b) the pressure at a point in the fluid domain.

abscissa along the junction. These functions are used to approximate the displacements and forces at the junctions for each uncoupled system α and to define the condensed transfer functions:

$$\mathbf{Y}^{\alpha}_{nm} = \left[\frac{\langle \bar{U}^{\alpha}_{m,q,p}, \varphi_n \rangle}{\langle F^{\alpha}_{m,q}, \varphi_m \rangle}\right]_{1\leq p\leq 4, 1\leq q\leq 4} = \left[\langle \bar{U}^{\alpha}_{m,q,p}, \varphi_n \rangle\right]_{p,q}, \tag{11}$$

where $\langle \bullet, \bullet \rangle$ is a scalar product. $\mathbf{F}^{\alpha}_{m}$ is the vector of the efforts on the junction, where the components in each direction of space is equal to φ_m. The indices p and q denote one of the four directions of space used in the case of a cylindrical shell (the three translations or forces and the rotation or moment around the tangential coordinate). $\bar{\mathbf{U}}^{\alpha}_{m,q}$ is the displacements vector of the junction when the subsystem is excited in the direction q by a force of magnitude $F^{\alpha}_{m,q}$.

Thanks to the superposition principle for linear passive systems, and to the forces equilibrium and displacements continuity, the coupling forces $\mathbf{F^c}$ between two subsystems α and β are deduced by the following equation:

$$\left(\mathbf{Y}^{\alpha} + \mathbf{Y}^{\beta}\right)\mathbf{F}^{c} = \tilde{\mathbf{U}}^{\beta} - \tilde{\mathbf{U}}^{\alpha} \tag{12}$$

where $\tilde{\mathbf{U}}^{\alpha} = \left[\langle \tilde{U}^{\alpha}_{p}, \varphi_n \rangle\right]_{n,p}$, is the vector of *free condensed displacements* and is calculated by projecting the displacement in the direction p on the condensation function φ_n when subsystem α is not coupled to the other subsystems and only excited by external forces.

Once the coupling forces have been calculated by inverting Eq. (12), the displacement at the point $\mathbf{x}$ of the coupled system can be deduced:

$$\mathbf{U}^{\alpha}(\mathbf{x}) = \tilde{\mathbf{U}}^{\alpha}(\mathbf{x}) + \sum_{n=1}^{N} \mathbf{Y}^{\alpha}_{\mathbf{x}n}\mathbf{F}^{c}_{n} \tag{13}$$

where $\tilde{\mathbf{U}}^{\alpha}(\mathbf{x})$ is the displacement at the point $\mathbf{x}$ when the subsystem α is uncoupled and excited by the external excitation. $\mathbf{Y}^{\alpha}_{\mathbf{x}n}$ is the condensed transfer function between the observation point $\mathbf{x}$ and the condensation

function φ_n (*i.e.* the displacement in $\mathbf{x}$ when the uncoupled subsystem is excited only by φ_n). Similarly, the pressure at the point $\mathbf{z}$ of the coupled system can be deduced:

$$p_{re}(\mathbf{z}) = \tilde{p}^{\alpha}_{re}(\mathbf{z}) + \sum_{n=1}^{N} \mathbf{Y}^{\alpha}_{\mathbf{z}n} \mathbf{F}^{c}_{n} \tag{14}$$

where $\tilde{p}^{\alpha}_{re}(\mathbf{z})$ is the pressure at the point $\mathbf{z}$ when the subsystem α is uncoupled and excited by the external excitation. $\mathbf{Y}^{\alpha}_{\mathbf{z}n}$ is the condensed transfer function between the observation point $\mathbf{z}$ and the condensation function φ_n.

The advantage of this method is that the condensed transfer functions of each uncoupled subsystem can be calculated by different techniques. In the case of a submerged cylindrical shell with internal structures, the submerged shell admittances are calculated through the Flügge equations, while the internal structures are modeled by Finite Elements.

The excitation of the coupled system is taken into account in the free displacement term, on the right hand side of Eq. (12). In the case of a point force, the free displacements of the shell can be calculated using the Füge equations and the free displacements of the internal frames can be determined using the FEM. Examples and validations on a complex submerged shell are given in [12]. In the case of an acoustical monopole, developments need to be done to calculate the free displacements of the shell. This is the aim of the next subsection.

3.2 Free displacements of the submerged shell for a monopole excitation

In the fluid domain surrounding the cylindrical shell, the pressure is decomposed as the sum of the blocked pressure p_b and the reradiated pressure p_{re} due to the system vibrations:

$$p = p_b + p_{re} \tag{15}$$

The blocked pressure will be used as a source term in the spectral equations of movement of the submerged cylindrical shell without internal structures [16]. The case of a monopole excitation outside the shell is considered, as seen in Fig. 2.

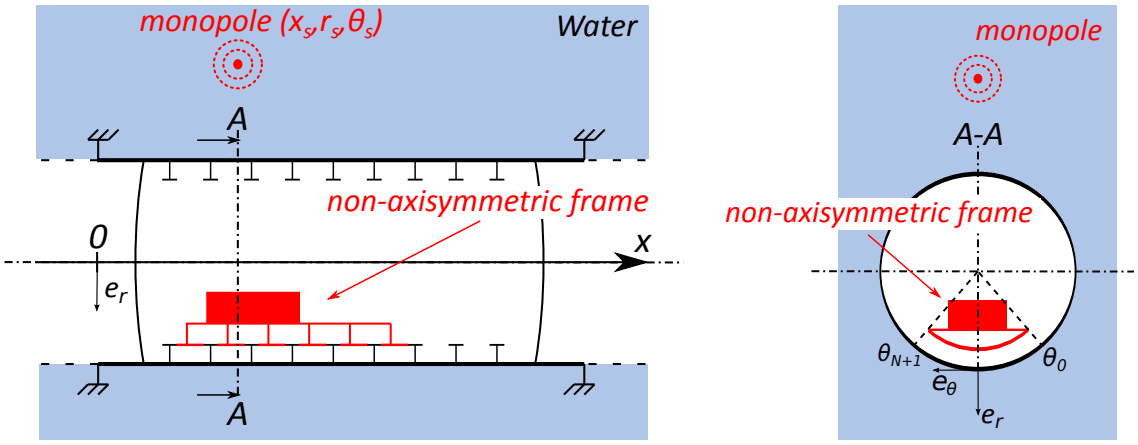

(a) (b)

Figure 2: Sections of a stiffened cylindrical shell model including a non-axisymmetric internal frame and an acoustic monopole in the fluid domain. (a) View in the plane $\theta = 0$. (b) View in the plane $x = x_A$.

The blocked pressure $p_b(x, r, \theta)$ is solution of the non-homogeneous Helmholtz equation:

$$\Delta p_b(x, r, \theta) + k_0^2 p_b(x, r, \theta) = q_{exc}(x, r, \theta) \tag{16}$$

where q_{exc} is the source term. The rigid boundary condition (Neumann) on the shell surface is written thanks to Euler's relation:

$$\frac{\partial p_b}{\partial r}(x, R, \theta) = 0 \tag{17}$$

with R the radius of the shell. The blocked pressure p_b is the sum of the incident pressure p_i and the scattered pressure p_s: $p_b = p_i + p_s$. The incident pressure is known and the scattered pressure needs to be calculated. From the previous equations, one can write:

$$\Delta p_s(x, r, \theta) + k_0^2 p_s(x, r, \theta) = 0 \tag{18}$$

and

$$\frac{\partial}{\partial r} p_s(x, R, \theta) = -\frac{\partial}{\partial r} p_i(x, R, \theta) \tag{19}$$

Applying a 2D-Fourier transform along the axial and tangential coordinates to Eq. (18) and (19) yields:

$$\frac{\partial^2}{\partial r^2}\tilde{\tilde{p}}_s(k_x, r, n) + \frac{1}{r}\frac{\partial}{\partial r}\tilde{\tilde{p}}_s(k_x, r, n) + \left(k_r^2 - \frac{n^2}{r^2}\right)\tilde{\tilde{p}}_s(k_x, r, n) = 0 \tag{20}$$

$$\frac{\partial}{\partial r}\tilde{\tilde{p}}_s(k_x, R, n) = -\frac{\partial}{\partial r}\tilde{\tilde{p}}_i(k_x, R, n) \tag{21}$$

where $\tilde{\tilde{p}}_s$ is the 2D-Fourier transform of the scattered pressure, and $k_r^2 = k_0^2 - k_x^2$. For a given k_x and n, Eq. (20) corresponds to Bessel's differential equation, which solutions can be written with Hankel's functions of the first and second kind of order n, $H_n^{(1)}$ and $H_n^{(2)}$ respectively:

$$\tilde{\tilde{p}}_s(k_x, r, n) = A_r H_n^{(1)}(k_r r) + B_r H_n^{(2)}(k_r r) \tag{22}$$

The constant A_r and B_r are calculated thanks to the Sommerfeld's radiation condition and the Euler's equation:

$$\begin{cases} A_r = & 0 \\ B_r = & -\frac{1}{k_r H_n^{(2)'}(k_r R)}\frac{\partial}{\partial r}\tilde{\tilde{p}}_i(k_x, R, n) \end{cases} \tag{23}$$

The incident pressure field for a monopole in (x_s, r_s, θ_s) can be expressed by:

$$p_i = p_0 \frac{e^{jk_0 d}}{d} \tag{24}$$

with $j^2 = -1$, p_0 the source intensity and d the distance between the source and the observation point. Applying a 2D-Fourier transform yields [17]:

$$\tilde{\tilde{p}}_i(k_x, r, n) = j\pi p_0 H_n^{(2)}(k_r r_s) J_n(k_r r) e^{-j(n\theta_s + k_x x_s)} \quad \text{for } r < r_s \tag{25}$$

Injecting Eq. (25) in Eq. (23) and then in Eq. (22) yields:

$$\tilde{\tilde{p}}_s(k_x, r, n) = -j\pi p_0 \frac{H_n^{(2)}(k_r r_s) J_n'(k_r R)}{H_n^{(2)'}(k_r R)} H_n^{(2)}(k_r r) e^{-j(n\theta_s + k_x x_s)} \tag{26}$$

The blocked pressure is deduced by summing the incident and scattered pressure:

$$\tilde{\tilde{p}}_b(k_x, R, n) = j\pi p_0 \left(J_n(k_r R) - \frac{H_n^{(2)}(k_r R) J_n'(k_r R)}{H_n^{(2)'}(k_r R)}\right) H_n^{(2)}(k_r r_s) e^{-j(n\theta_s + k_x x_s)} \tag{27}$$

Using that $J_n(z) H_n^{(2)'}(z) - J_n'(z) H_n^{(2)}(z) = -\frac{2j}{\pi z}$, Eq. (27) can finally be written as:

$$\tilde{\tilde{p}}_b(k_x, R, n) = \frac{2p_0}{k_r R} \frac{H_n^{(2)}(k_r r_s)}{H_n^{(2)'}(k_r R)} e^{-j(n\theta_s + k_x x_s)} \tag{28}$$

This expression can be used in the right-hand term of the spectral Flügge equations to determine the free displacements of the shell under a monopole excitation. This method is applied in the next section to discuss the influence of the internal structures on the vibroacoustic behavior of a submerged shell under a random excitation.

4. TEST CASE APPLICATION

4.1 Description of the system

A 5 m radius, 42.3 m length and 30 mm thick cylindrical shell stiffened with 51 stiffeners and 2 spherical bulkheads (10 mm thick, 30 m curvature radius) is considered in this section, as shown in Fig. 3a. There are three different types of stiffeners and their spacing varies between 0.6 and 1 m. The whole system is made of steel ($\eta = 0.02$) and is immersed in water. Clamped boundary conditions are used at the ends of the shell, 2 m away from the first and the last stiffeners. A non-axisymmetric frame is linking the two stiffeners at $x = 11.5$ m and $x = 21.5$ m. A model of this internal structure is shown in Fig. 3b, with the colors representing the displacement magnitude of the eigenmode at 170 Hz. It consists in a plate assembly made of a horizontal floor, a vertical stiffening plate and two disc sections that are linked to the stiffeners. Displacements continuity is assumed at all the junctions.

In order to use the reciprocity principle, a point force is applied on the surface of the cylindrical shell at the point M_1 of coordinates $(x, \theta, r) = (11.5, 0, 5)$. Similarly, a monopole excitation is defined at the point M_2 of coordinates $(x, \theta, r) = (11.5, 0, 500)$. The response of the system is calculated through the CTF method for both excitations separately, and thanks to the reciprocity principle, the sensitivity functions are given by the response in the wavenumber-frequency space.

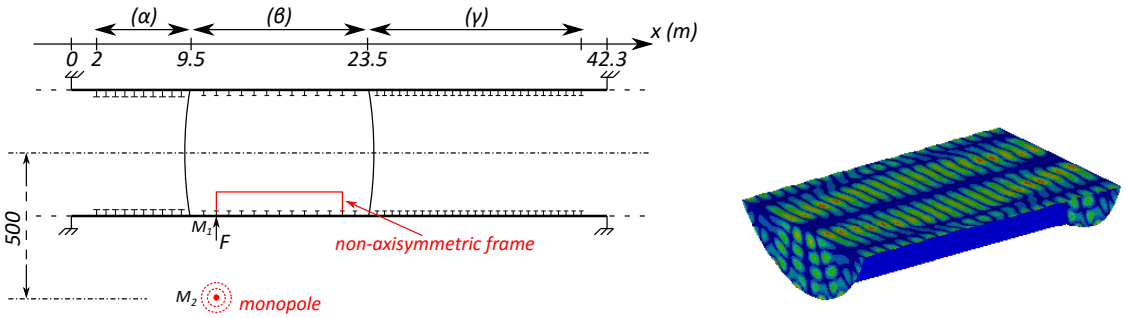

(a) (b)

Figure 3: Submerged cylindrical shell with axisymmetric stiffeners: (α) spacing 0.75 m, T-cross-section (mm): $300 \times 60/60 \times 300$; ($\beta$) spacing 1 m, T-cross-section (mm): $200 \times 15/15 \times 200$; ($\gamma$) spacing 0.6 m, T-cross-section (mm): $200 \times 25/15 \times 200$. (a) Section in the plane $\theta = 0$. (b) Mode at 170 Hz of the non-axisymmetric frame.

4.2 Examples of sensitivity functions

Sensitivity functions, *i.e.* accelerations of the shell in the wavenumber space, are calculated thanks to the CTF method under the point force and under the monopole excitation. The results are plotted in Fig. 4 for the point force at $f = 207$ Hz and in Fig. 5 for the monopole excitation at $f = 568$ Hz.

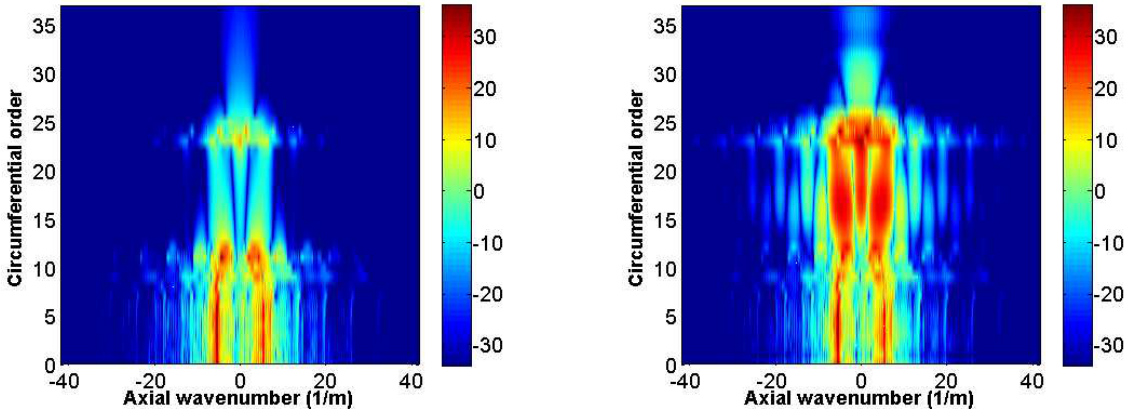

(a) (b)

Figure 4: Sensitivity function (acceleration in dB ref gμm.s^{-2}) in the wavenumber space for a point force at M_1 at $f = 207$ Hz. (a) Axisymmetric case. (b) Non-axisymmetric case.

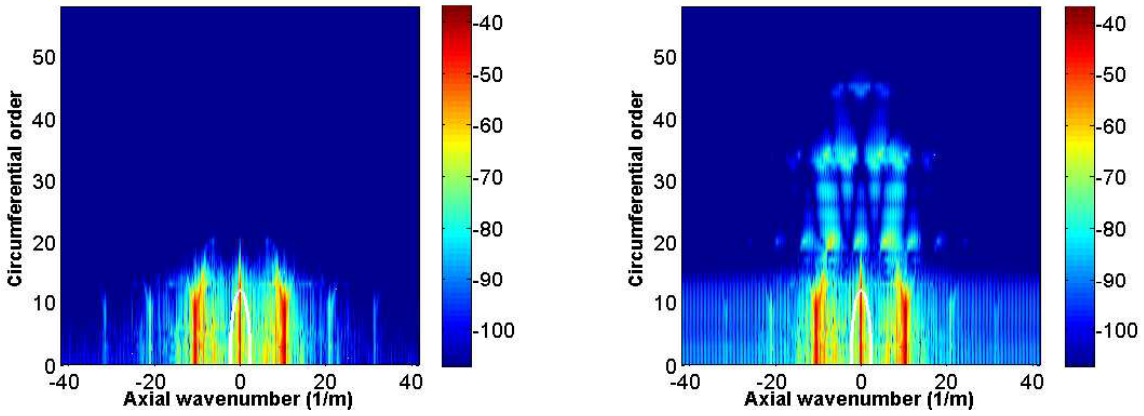

(a) (b)

Figure 5: Sensitivity function (acceleration in dB ref gμm.s^{-2}) in the wavenumber space for a monopole at M_2 at $f = 568$ Hz. (a) Axisymmetric case. (b) Non-axisymmetric case.

These frequencies are chosen because differences can clearly ben seen in the spectra. Indeed, more circumferential orders tend to play a role in the response of the structure when there is a non-axisymmetry [12, 18]. In Fig. 5, the white line represents the radiation circle. The spectral components inside this circle are the main contributors to the pressure radiated in the far-field [19]. No clear difference can be seen inside the radiation circle at this frequency, so no large difference is expected in the power spectral density of the pressure at M_2.

4.3 Diffuse Sound Field

As the radius of curvature of the shell is large compared with the wavelength, the expression of a diffuse sound field (DSF) for a plate in the wavenumber-frequency space is taken as [20]:

$$\phi_{pp}(k_x, k_\theta, f) = \begin{cases} \frac{\pi}{k_0} \frac{S_{pp}(f)}{\sqrt{k_0^2 - (k_x^2 + k_\theta^2)}} & \text{if } \sqrt{k_x^2 + k_\theta^2} < k_0^{in} \\ 0 & \text{if } \sqrt{k_x^2 + k_\theta^2} \geq k_0^{in} \end{cases} \tag{29}$$

with S_{pp} the frequency spectral density, taken constant equal to 1 Pa^2.s in this example. $k_0^{in} = \frac{2\pi f}{c_0^{in}}$ is the acoustic wavenumber. As air is considered inside the cylindrical shell (with weak coupling only), the sound velocity is $c_0^{in} = 340$ m.s^{-1}.

In this example, the DSF excites only the cylinder on the section between the two bulkheads at $x = 9.5$ and $x = 23.5$ m. According to the reciprocity principle and to Eq. (10), it consists in calculating the displacements of the structure under a point force at $\mathbf{x}$ only on $\tilde{\mathbf{x}} \in \Sigma_p$.

Fig. 6 shows the power spectral densities of the radial acceleration at M_1 and pressure at M_2 as a function of the frequency with and without the non-axisymmetric internal frame. The red solid line shows the results in the case of the axisymmetric stiffened shell (*i.e.* the stiffened submerged shell without the internal frame) and the blue dashed line shows the case where the non-axisymmetric frame is taken into account. It can be said that the non-axisymmetric internal frame has an influence on the response of the structure when it is excited by the DSF. For the acceleration at M_1, the power spectral density tends to decrease except for some frequency ranges. The decrease can be explained from the reciprocity principle, by saying that the amplitude of displacement is on average lower in the non-axisymmetric case [12, 21]. The increases can be explained by looking at the sensity functions shown in Fig. 4 where more circumfenential orders play a role in the non-axisymmetric case. For the power spectral density of pressure at M_2, an increase smaller than 2 dB can be seen.

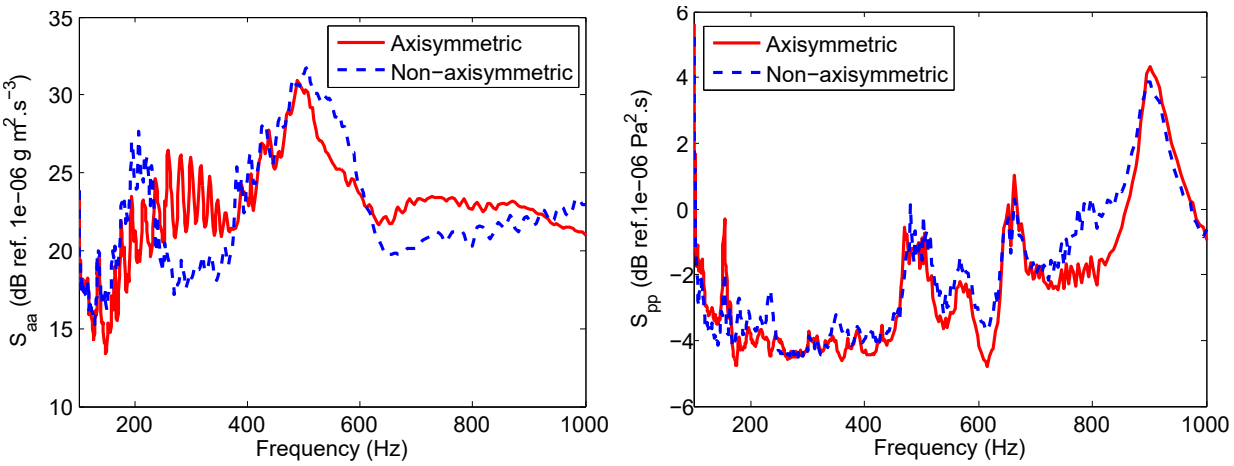

(a) (b)

Figure 6: Power spectral density of the system excited by a diffuse sound field with and without the non-axisymmetric internal structure as a function of the frequency of the (a) radial acceleration at M_1 and (b) pressure at M_2.

4.4 Turbulent Boundary Layer excitation

A structure immersed in a flow can be excited by a Turbulent Boundary Layer which is characterized by the parameters shown in Table 1 [22]. These parameters can be calculated through CFD (computational fluid dynamics) calculations. This is however not the aim of the present work and the values have thus been arbitrarily chosen for naval applications, and used in simple models to calculate the wavenumber-frequency spectrum of the wall pressure.

Table 1: Turbulent Boundary Layer parameters

Parameter	Notation	Value
Flow speed	U_∞	15 m.s^{-1}
Friction velocity	U_T	1 m.s^{-1}
Thickness	δ	0.01 m
Kinematic viscosity (at 20°C)	ν_0	1.005 μ Pa.s
Fluid density	ρ_0	1000 kg.m^{-3}

The strongest pressure fluctuations occur at the convective wavenumber k_c and the acoustic wavenumber k_0 defined by:

$$k_c = \frac{2\pi f}{U_c} \text{ and } k_0 = \frac{2\pi f}{c_0} \tag{30}$$

where U_c is the convection speed taken as $U_c = 0.6U_\infty$ [22, 23] and $c_0 = 1500$ m.s^{-1}. The acoustic, convective and flexural wavenumbers are plotted as a function of the frequency up to 1000 Hz in Fig. 7a. The flexural wavenumber is calculated for a $h = 0.03$ m thick plate made of steel (density $\rho_s = 7800$ kg.m^{-3}, Young modulus $E = 210$ GPa and Poisson coefficient $\nu = 0.3$) through the following formula [24]:

$$k_f = \sqrt{\frac{2\pi f}{h}} \left(\frac{12(1-\nu^2)\rho_s}{E} \right)^{1/4} \tag{31}$$

It can be seen in Fig. 7a that the convective wavenumber is much bigger than the acoustic and flexural wavenumbers for the parameters chosen for this study. On the other hand, the radial accelerations of a cylinder above the ring frequency, $f_r = \frac{1}{2\pi R}\sqrt{\frac{E}{\rho_s(1-\nu^2)}} = 173$ Hz, present generally maxima for wavenumbers around the flexural wavenumber and then decreases when the wavenumber increases. Fig. 7b shows the module of the radial acceleration as a function of the axial wavenumber for the circumferential order $n = 0$ at the frequency $f = 1000$ Hz. It clearly shows that the amplitude is maximum at the flexural wavenumber k_f, and then drops dramatically. It can thus be said that the structure acts as a filter on the high wavenumbers

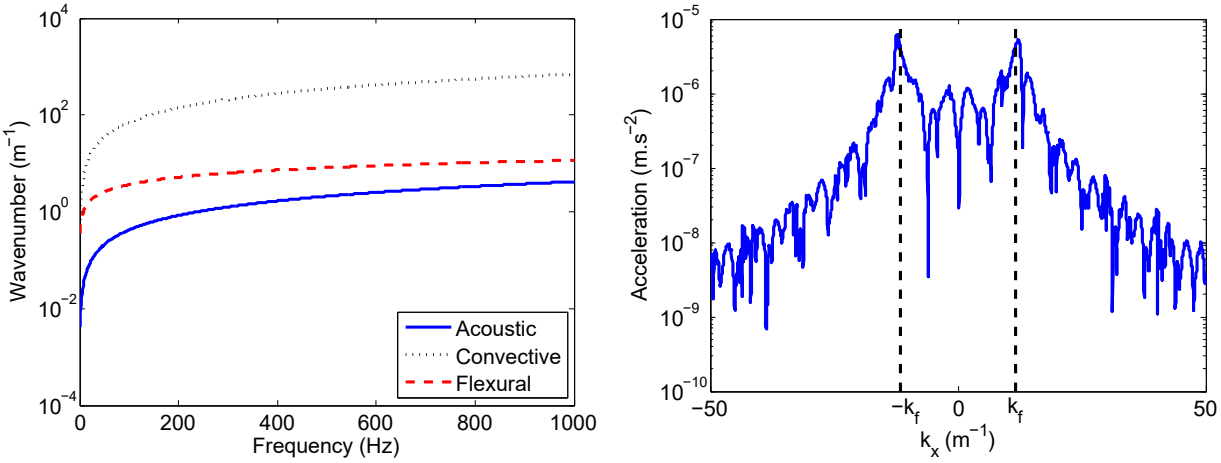

(a) (b)

Figure 7: (a) Acoustic (blue solid line), convective (black dotted line) and flexural (red dashed line) wavenumbers as a function of the frequency. (b) Radial acceleration as a function of the axial wavenumber k_x at 1000 Hz for the circumferential order $n = 0$ and for a point force at M_1

and that the vibrations are mainly due to the acoustic components of the TBL. As mentionned at the end of section 2, a cutoff wavenumber $\mathbf{N_k}$ can thus be defined from the flexural waenumber and a margin coefficient to numerically calculate the integrals of Eqs. (7) and (8). In this example, the margin coefficients are taken equal to 4 for the axial wavenumbers and 1.2 for the circumferential wavenumbers.

In the present study, the wavenumber-frequency of the wall pressure $\phi_{pp}(k_x, k_\theta, f)$ is expressed as:

$$\phi_{pp}(k_x, k_\theta, f) = S_{pp}(f)\Psi_{pp}(k_x, k_\theta, f) \tag{32}$$

An empirical model proposed by Goody [25] is used for the frequency spectral density $S_{pp}(f)$:

$$S_{pp}(f) = \frac{4\pi C_2 \tau_w^2 (2\pi f)^2 \delta^3}{U_\infty^3 \left(\left[C_1 + \left(\frac{2\pi f \delta}{U_\infty} \right)^{0.75} \right]^{3.7} + \left[C_3 R_T^{-0.57} \left(\frac{2\pi f \delta}{U_\infty} \right) \right]^7 \right)} \tag{33}$$

where C_1, C_2 and C_3 are respectively 0.5, 1.5 and 1.1. $R_T = \frac{U_T^2 \delta}{\nu_0 U_\infty}$ is the Reynolds number that takes into account the ratio of intertial forces to viscous forces. $\tau_w = \rho_0 U_T^2$ is the shear constraint at the wall. The cross-spectrum $\Psi_{pp}(k_x, k_\theta, f)$ is deduced from a spatial Fourier Transform of the expression given by Corcos [7] and yields:

$$\Psi_{pp}(k_x, k_\theta, f) = \frac{4\alpha\beta}{\left[\left(k_x - \frac{2\pi f}{U_c} \right)^2 + \left(\frac{2\pi f \alpha}{Uc} \right)^2 \right] \left[k_\theta^2 + \left(\frac{2\pi f \beta}{Uc} \right)^2 \right]} \tag{34}$$

with $\alpha = 0.11$ and $\beta = 0.77$ empirical values.

The power spectral density of the acceleration at M_1 and of the pressure at M_2 are plotted as a function of the frequency in Fig. 8a and 8b respectively. Similarily to the results from the diffuse sound field, it can be said that the non-axisymmetric internal frame has an influence on the response of the system when it is excited by a TBL. Differences up to 6 dB can be seen in Fig. 8a for the power spectral density of acceleration at M_1 between the axisymmetric and non-axisymmetric cases . For the power spectral density of pressure at M_2 shown in Fig. 8b, the differences between the two cases are smaller. No clear difference can be seen below 250 Hz, and the non-axisymmetric case is between 1 and 2 dB higher in the rest of the frequency range.

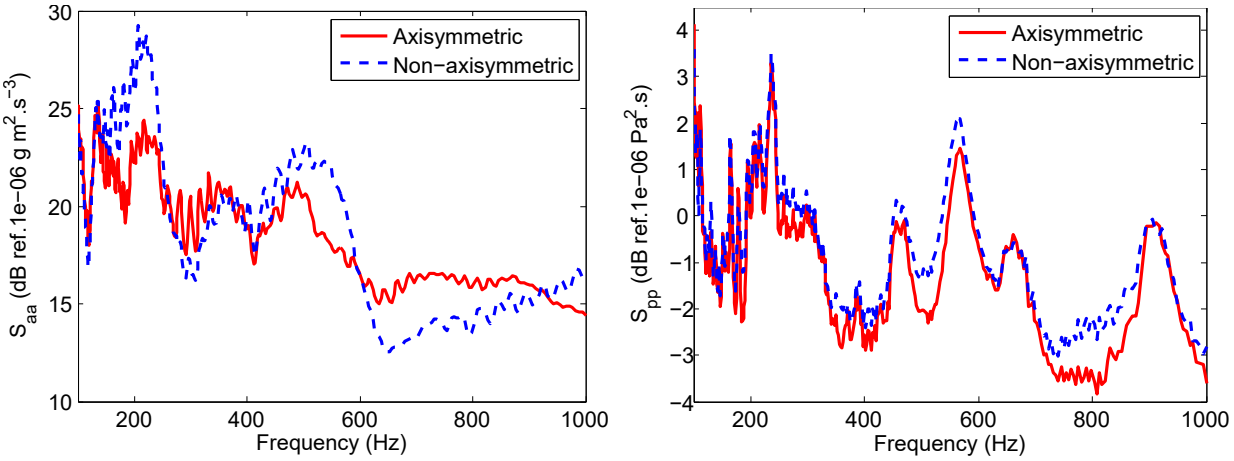

(a) (b)

Figure 8: Power spectral density of the system excited by a turbulent boundary layer with and without the non-axisymmetric internal structure as a function of the frequency of the (a) radial acceleration at M_1 and (b) pressure at M_2.

5. CONCLUSION

The response of a submerged stiffened cylindrical shell with non-axisymmetric internal frames under random excitations has been calculated. For this purpose, the wavenumber-frequency (k, M) reciprocity technique has been presented and is based on sensitivity functions, that are the result of deterministic calculations of the system under a point force or a monopole. They are estimated with the CTF method, that is a substructuring method that enables to take internal frames in a submerged shell into account. One of the main advantage of this approach is that once the sensitivity functions are stored in a database, it is easy to change the excitation by modifying the expression of the wall pressure spectrum ϕ_{pp}.

An application on a test case taken from the naval industry under different random excitations (DSF, TBL) shows the versatility of the method. From the results it can be said that the non-axisymmetric internal frames can have an influence on the response of the system under random excitations. As more circumferential orders tend to play a role when the system is non-axisymmetric, the response tends to be higher in this case. The method can now be used to further investigate physical phenomena (Bloch-Floquet waves propagation for instance) involved in a stiffened submerged cylindrical shell under random excitation.

ACKNOWLEDGMENTS

This work was funded by DCNS and performed within the framework of the LabEx CeLyA of Université de Lyon, operated by the French National Research Agency (ANR-10-LABX-0060/ANR-11-IDEX-0007).

REFERENCES

[1] W. A. Strawderman. Turbulence-induced plate vibrations: an evaluation of finite-and infinite-plate models. *The Journal of the Acoustical Society of America*, 46(5B):1294–1307, 1969.

[2] W. A. Strawderman and R. A. Christman. Turbulence-induced plate vibrations: Some effects of fluid loading on finite and infinite plates. *The Journal of the Acoustical Society of America*, 52(5B):1537–1552, 1972.

[3] M. Aucejo. *Vibro-acoustique des structures immergées sous écoulement turbulent*. PhD thesis, INSA de Lyon, 2010.

[4] M. L. Rumerman. Estimation of broadband acoustic power radiated from a turbulent boundary layer-driven reinforced finite plate section due to rib and boundary forces. *The Journal of the Acoustical Society of America*, 111(3):1274–1279, 2002.

[5] L. Maxit and V. Denis. Prediction of flow induced sound and vibration of periodically stiffened plates. *The Journal of the Acoustical Society of America*, 133(1):146–160, 2013.

[6] W. A. Strawderman. Wavevector-frequency analysis with applications to acoustics. Technical report, DTIC Document, 1994.

[7] G. M. Corcos. Resolution of pressure in turbulence. *The Journal of the Acoustical Society of America*, 35(2):192–199, 1963.

[8] D. M. Chase. The character of the turbulent wall pressure spectrum at subconvective wavenumbers and a suggested comprehensive model. *Journal of Sound and Vibration*, 112(1):125–147, 1987.

[9] W. K. Blake. Aero-hydroacoustics for ships, vol. ii. Technical report, DTNSRDC-84/010, David W. Taylor Naval Ship Research and Development Centre, Bethesda, 1984.

[10] Richard M Lueptow. Turbulent boundary layer on a cylinder in axial flow. Technical report, DTIC Document, 1988.

[11] V. Meyer, L. Maxit, J.-L. Guyader, T. Leissing, and C. Audoly. A condensed transfer function method as a tool for solving vibroacoustic problems. *Proc IMechE Part C: J Mechanical Engineering Science*, 230(6):928–938, 2016.

[12] V. Meyer, L. Maxit, J.-L. Guyader, and T. Leissing. Prediction of the vibroacoustic behavior of a submerged shell with non-axisymmetric internal substructures by a condensed transfer function method. *Journal of Sound and Vibration*, 360:260–276, 2016.

[13] F. A. Firestone. The mobility method of computing the vibration of linear mechanical and acoustical systems: Mechanical-electrical analogies. *Journal of applied Physics*, 9(6):1788–1794, 2004.

[14] L. Maxit. Wavenumber space and physical space responses of a periodically ribbed plate to a point drive: A discrete approach. *Applied acoustics*, 70(4):563–578, 2009.

[15] F. J. Fahy. Some applications of the reciprocity principle in experimental vibroacoustics. *Acoustical Physics*, 49(2):217–229, 2003.

[16] L. Maxit and J.-M. Ginoux. Prediction of the vibro-acoustic behavior of a submerged shell non periodically stiffened by internal frames. *The Journal of the Acoustical Society of America*, 128(1):137–151, 2010.

[17] E. A. Skelton and J. H. James. Acoustics of an anisotropic layered cylinder. *Journal of sound and vibration*, 161(2):251–264, 1993.

[18] M. H. Marcus and B. H. Houston. The effect of internal point masses on the radiation of a ribbed cylindrical shell. *The Journal of the Acoustical Society of America*, 112(3):961–965, 2002.

[19] E. G. Williams, B. H. Houston, and J. A. Bucaro. Experimental investigation of the wave propagation on a point-driven, submerged capped cylinder using k-space analysis. *The Journal of the Acoustical Society of America*, 87(2):513–522, 1990.

[20] C. Marchetto, L. Maxit, O. Robin, and A. Berry. Caractérisation expérimentale de structures sous champ acoustique diffus : mesure des fonctions de sensibilité par principe de réciprocité. CFA/VISHNO 2016, Le Mans, France, 2016.

[21] V. Meyer, L. Maxit, J.-L. Guyader, C. Audoly, and Y. Renou. Vibrations et rayonnement acoustique des coques cylindriques raidies : étude expérimentale de l'influence des structures internes non-axisymétriques. CFA/VISHNO 2016, Le Mans, France, 2016.

[22] M. S. Howe. Surface pressures and sound produced by turbulent flow over smooth and rough walls. *The Journal of the Acoustical Society of America*, 90(2):1041–1047, 1991.

[23] B. Arguillat, D. Ricot, C. Bailly, and G. Robert. Measured wavenumber: Frequency spectrum associated with acoustic and aerodynamic wall presure fluctations. *The Journal of the Acoustical Society of America*, 128(4):1647–1655, 2010.

[24] M. C. Junger and D. Feit. *Sound, structures, and their interaction*, volume 240. MIT press Cambridge, MA, 1972.

[25] M. Goody. Empirical spectral model of surface pressure fluctuations. *AIAA journal*, 42(9):251–264, 1993.